PORCINO D, Marcianò V. (2017). Bonding Degradation and Stress-Dilatancy Response of eakly Cemented Sands. *GEOMECHANICS AND GEOENGINEERING*, vol. , 12(4), 221-233, ISSN: 1748-6025, doi: 10.1080/17486025.2017.1347287

Geomechanics and Geoengineering: an International Journal

ARTICLE TYPE : RESEARCH PAPER

Article Title: "BONDING DEGRADATION AND STRESS–DILATANCY RESPONSE OF WEAKLY CEMENTED SANDS"

Authors : Daniela D. Porcino [1] &Vincenzo Marcianò[2]

[1] *Associate Professor in Geotechnical Engineering, Department DICEAM, University "Mediterranea" of Reggio Calabria, Via Graziella (Feo di Vito)-89060 Reggio Calabria, Italy. E-mail:daniela.porcino@unirc.it.*

[2] *Doctor of Philosophy in Geotechnical Engineering, Department DICEAM, University "Mediterranea" of Reggio Calabria, Via Graziella (Feo di Vito)-89060 Reggio Calabria, Italy, e-mail: vincenzo.marciano@unirc.it*

BONDING DEGRADATION AND STRESS–DILATANCY RESPONSE OF WEAKLY CEMENTED SANDS

D.D.Porcino & V. Marcianò

Abstract

The progressive bond breakage of artificially cemented sands induced by shear straining was investigated through conventional isotropically consolidated drained triaxial compression tests. Sand specimens were prepared with a low degree of cementation by adopting a chemical grout. Test results were interpreted in terms of the stress-dilatancy theories for cohesive-frictional materials proposed by Rowe (1962) and Zhang and Salgado (2010). The influence of debonding on the stress-dilatancy behaviour of cemented sands was analyzed with particular emphasis on the "delayed dilatancy" phenomenon. A bonding degradation curve was determined for each test relating the interparticle cohesion (c) to the magnitude of the total plastic strain vector (ε_d) and a bond degradation rate factor (D_c) was assessed from each curve. The maximum value of interparticle cohesion (c_o) before the onset of bond degradation under shearing, was found to correspond with a sharp decrease in the soil stiffness of the specimens. The influence of the effective confining stress (p'_c) on both c_o and D_c parameters gathered from each test was also ascertained.

1. Introduction and literature review

Studies concerning the mechanical behaviour of naturally cemented soils are not straightforward and can give inconsistent results due to the high variability of these materials. The difficulties increase significantly when one is concerned with weakly to moderately cemented soils due to their enhanced sensitivity to even small disturbance effects induced by in situ sampling and laboratory operations. It has been recognized (Leroueil and Vaughan 1990, Lo et al. 2003, Vaughan 1985) that cemented soils exhibit similar patterns of stress-strain behaviour irrespective of the nature and strength of the cementing agents. According to this evidence, experimental research works conducted on artificially cemented soils have been used to investigate basic features of the mechanical behaviour of naturally bonded geomaterials. These works include several cementing agents adopted in conventional grouting treatments such as Portland cement, calcite, fly ash, gypsum, silicate based solutions, etc. (Clough and Sitar 1981, Consoli et al. 2012, Coop and Atkinson 1993, Cuccovillo and Coop 1997,199, Huang and Airey 1993, Ismail et al. 2002, Lade and Overton 1989, Marri et al. 2012, Porcino et al. 2012, Reddy and Saxena1993, Rios et al. 2014, Rotta et al. 2003, Schnaid et al. 2001, Wang and Leung 2008b). Results obtained evidenced some common features of their behaviour, highlighting the need to define a consistent and unified conceptual framework for the analysis of the complex mechanical behaviour of these materials (Cuccovillo and Coop1999, Gens and Nova 1993, Vatsala et al.2001). Among them, the most peculiar phenomena are bonding degradation and related post-yielding deformational pattern. Inside the initial (or bond) yield locus, whose size is related to the amount and strength of the deposited cement, the cementing agent imparts to the soil skeleton an extra strength which enables it to sustain the applied stresses at void

ratios higher than those exhibited by the corresponding uncemented soils. Furthermore, bonding also imparts the sample a tensile strength which can be conveniently represented by the unconfined compressive strength, as demonstrated by a linear relationship between unconfined compressive strength and cement content in laboratory experiments carried out by Schnaid et al. (2001). However, in lightly cemented sands, due to the weak nature of the bonds, the tensile strength is often very difficult to be assessed.

Cementation enhances rigidity of the soil skeleton which undergoes predominantly elastic ("recoverable") strains. Dilative strains that are plastic in nature are not allowed at this stage. After yielding, both in compression and shearing, stress-strain curves deviate from the initial elastic trend allowing yield points to be detected by visual inspection of curves. Positive examples, in which it was relatively easy to identify yield loci, have been reported in literature (Consoli et al. 2012, Cuccovillo and Coop 1993, Schnaid et al. 2001). Such examples were generally concerned with moderate to heavily cemented soils where the cementing agent fills significant portions of the original interparticle voids. It should be noted, however, that a limited amount of research on weakly cemented soils is present in literature (e.g. Lo et al. 2003, Wang and Leung 2008b) although only some of this research presents data concerning yield loci (Coop 2005, Cuccovillo and Coop 1999).

Wang and Leung (2008a and 2008b) combined triaxial test results with numerical simulations using discrete element method (DEM) to analyze the influence of debonding on the stress-dilatancy behaviour of a weakly cemented sand. After a very early stage of shearing, in which a limited amount of compressive strains was observed, plastic dilative strains started to occur at a progressively increasing dilation rate. Contrary to what was traditionally observed on uncemented sands, the

maximum dilation rate was reached beyond the peak strength ("delayed dilatancy"). An explanation of this feature is reported in Wang and Leung (2008a and 2008b) and it is also presented in par. [3.2] of this paper.

Based on experimental evidence gathered from triaxial tests carried out at zero effective confinement stress (p'_c=0), Lo et al.(2003) demonstrated that the deviatoric peak stresses mobilized in such tests correspond to a fully cohesive (i.e. non dilative) shear strength. More recently, there has been a great deal of interest in the formulation of theoretical models capable of capturing the main features of the behaviour of bonded geomaterials. It has been recognized that most of these features can be analyzed in the frame of the concepts of critical state soil mechanics and elasto-plasticity theories, provided that appropriate modifications are introduced in the existing constitutive models developed for unbonded geomaterials (Baudet and Stallebrass 2004, Gens and Nova 1993, Nova et al. 2003, Lagioia and Nova 1995, Rouainia and Wood 2000, Yu at al. 2005, 2007). Key issues of proposed models are: a) the parameter adopted to describe the strength of cement bonds at any stage of the loading process, and b) the relationship adopted to describe bond degradation with plastic strains (Gens and Nova 1993).

Formulation of stress-dilatancy theories in terms of energy has helped to ascertain that the mobilized strength of a bonded geomaterial in triaxial testing conditions is mainly the result of the contribution of three components, namely: the friction at critical state, dilatancy, and the energy used in the bond breakages or destructuration, which is related to the mobilized cohesion component (Cuccovillo and Coop1999, Lade and Overton 1989, Rowe 1962,1963, Wang and Leung 2008b). In Rowe's formulation of stress-dilatancy theory (1962,1963), the last parameter is expressed by the interparticle cohesion (c). Yu at al.(2007) proposed an unified

critical state model (CASM-n) in which Rowe's stress-dilatancy relationship, developed for cohesive-frictional materials, is adopted as a non-associative flow rule for describing the plastic flow of bonded geomaterials. The progressive bonding degradation taking place during shearing is assumed to be a strain dependent phenomenon and a relationship between the interparticle cohesion and the total plastic strain (defined as magnitude of the resultant vector of both volumetric and deviatoric strain components) is provided. As in previous research (e.g. Gens and Nova 1993), an exponential law is tentatively assumed. Actually, this assumption needs to receive a deeper confirmation based on a more varied set of experimental data.

Zhang and Salgado (2010) derived a new stress-dilatancy relationship for cemented materials using a saw-tooth model and laws of friction adopted by De Josselin de Jong (1976). In a previous study, Lade and Overton (1989) investigated the stress-strain behaviour of cemented sands following an approach based on Caquot's stress transformation principle. The results obtained were consistent with those presented successively by Zhang and Salgado (2010).

The purpose of this paper is to present an experimental investigation on bonding degradation during shearing phase of weakly cemented sands with particular emphasis on stress-dilatancy behaviour and strength features before and after peak state. Test results were analyzed in the context of theoretical stress-dilatancy relationships for cohesive-frictional materials, with the assumption that the interparticle bonding is not constant during shearing.

2. Materials tested and testing procedures

Conventional triaxial drained monotonic compression tests were performed on

specimens of uncemented and cemented soil samples. A natural sand, namely Ticino sand (TS), was used in this study and improved by a silicate-based solution (Porcino et al. 2011, 2012), capable of imparting a weak level of cementation. Physical properties of tested sand are reported in table 1. Preparation of cemented samples comprised: reconstitution of sand specimen by air pluviation, pre-saturation and grouting phase. Details of treated sample preparation and the adopted system are reported in previous papers published by the authors (Porcino et al. 2011, 2012). Cylindrical cemented specimens, 70 mm in diameter and 140 mm in height, with a target initial void ratio corresponding to a loose state were then prepared for triaxial testing. In the case of weakly cemented samples, the preparation of homogeneous uniformly grouted samples requires minimizing disturbance effects caused by curing conditions, extrusion, sampling or trimming operations. This was achieved by adopting a longitudinally-split mould with a diameter and height corresponding to those of cemented tested samples. This aspect is critical for lightly cemented grouted samples such as those tested in the present study.

The samples were installed in the triaxial chamber immediately after the curing time, and isotropically consolidated under different effective confining pressures (p'_c). Uncemented and cemented samples were tested under low (20 kPa) to medium (200 kPa) isotropic confining pressures; in some cases the samples were tested under higher stress levels (up to 400 kPa). The saturation phase for cemented samples in triaxial apparatus was realized by applying a back-pressure equal to 300 kPa for a period of 12 hours. At the end of saturation, Skempton's parameter B was measured and values of 0.95 were obtained. Afterwards, specimens were isotropically consolidated under the desired mean effective stress. Drained shearing was finally applied at a constant displacement rate of 0.030 mm/min. In this apparatus, the

volume variation was monitored by an automated volume measurement system, while the axial load was measured by an internal submersible load cell with a maximum capacity of 5000 N and accuracy ± 0.05% l.c. Axial displacement was measured with a Linear Variable Differential Transformer (LVDT). All measurements attained accuracies exceeding the requirements of ASTM D 4767-11. Most drained tests were taken up to large strains (25-30% axial strain) in order to reach ultimate state conditions. The results of preliminary unconfined compression triaxial tests performed on lightly cemented sand samples provided mean values of unconfined compression strength (q_{UCS}) equal to 75 kPa.

In the present study, for the purpose of comparison, additional drained TX test results performed on moderately cemented specimens of the same sand were presented with the aim of evidencing some peculiar features of weakly cemented sands, or verifying some proposed procedures. Artificial cementation was induced by adopting a commercial mineral–based grout ("Silacsol") resulting in moderately treated sand specimens with a mean value of unconfined compression strength q_{UCS} equal to 500 kPa (Porcino et al., 2015).

3. Analysis of test results

3.1 Isotropic compression and shearing behaviour

Data from isotropic triaxial compression tests carried out on both cemented and uncemented sands are shown in the ε_{vol} (volumetric strain):ln p' plane of figure 1.

The yield of the weakly cemented sand is not distinctly identified but closer examination of the tangent bulk modulus vs p' curve reveals an elastic initial behaviour up to a threshold of mean effective stress (p'_y) close to 40 kPa. As illustrated in fig 1a, yield occurs inside the intrinsic normal compression line of

uncemented reconstituted sand; according to Coop (2005), this feature is indicative of a “weak” cementation.

Under drained monotonic shearing, typical patterns of response for the weakly bonded sand are illustrated in fig. 1b. As can be seen, when the soil is sheared at confining pressures p_c'=20 kPa below the isotropic yield stress, an evident peak in the stress ratio (η)-axial strain (ε_a) curve occurs at small strains that corresponds to a fully cohesive (i.e. non dilative) peak strength. On the other hand, when the confining stress exceeds the yield stress in compression (p'_c= 200 kPa), the peak tends to disappear and the shearing behaviour is similar to that observed for an equivalent uncemented soil (i.e. a predominanty frictional behaviour).

The complete set of data gathered from all TX tests conducted on both uncemented and weakly cemented sand specimens are presented in figures 2 and 3, respectively. In particular, the deviatoric stess ($q = \sigma_1 - \sigma_3$) vs. axial strain (ε_a) curves and volumetric strain (ε_{vol}) vs. axial strain ($\boldsymbol{\varepsilon_a}$) curves of uncemented sand at different effective confining stresses, are plotted in figure 2. Comparing the behaviour of cemented sand samples (fig. 3) with that exhibited by the uncemented ones (fig.2) reveals that, at low confining stresses, cementation significantly alters the volumetric response of cemented sands enhancing their dilative behaviour. As can be argued, cemented soils exhibit a gradual evolution from a brittle strain softening behaviour dominated by cement bonds at low confining stresses, towards a more gentle strain softening behaviour at elevated confining stresses. A distinct strain-softening response was accompanied by strain localization (usually in the form of a dominant shear band) and it became visible after the peak strength, at approximately the stage when the maximum dilation rate occurred. With increasing initial cement strength (i.e. moderately cemented sands), diagonally crossing shear bands occurred.

3.2 Stress-dilatancy and Strength Characteristics

Figure 4a shows the plot of stress-dilatancy behaviour for an artificially weakly cemented sample of TS which was derived from drained triaxial test data performed at low effective confining stress (i.e. 20 kPa). Also the stress-dilatancy curve for a moderately cemented sample of the same sand sheared at the same mean effective confining stress is reported in the same figure for comparison purposes (fig. 4b). The dilatancy, *d (*(dilation plotted as negative in the figure), is defined as $d = \frac{\delta\varepsilon_p^p}{\delta\varepsilon_q^p}$ where: $\delta\varepsilon_p^p$ and $\delta\varepsilon_q^p$ are the incremental plastic volumetric and deviatoric strains, respectively. It should be noted that, for simplicity, total strains are plotted here. Nonetheless, the elastic component after the soil had yielded is relatively small. Before yielding, an elastic response of the overall structure is maintained since plastic response and associated dilatancy are inhibited by cementation (Wang and Leung (2008b). The relative portions of curves in fig 4 are outside the range of applicability of stress-dilatancy theories. In both cases (weakly and moderately cemented sands), some peculiar features of the stress-dilatancy behaviour of bonded materials can be highlighted.

In agreement with other researchers (Coop & Willson 2003, Cuccovillo and Coop 1997, Hamidi and Haeri 2008, Lo et al. 2003, Malandraki and Toll 2001, Schnaid et al. 2001) the authors defined two yield points in shearing (respectively a “first” and a “gross” yield point) corresponding to the two sequential dropping points observed on the tangent stiffness *vs.* strain curve, drawn in double logarithmic space (fig.5). The onset of breakage of the weakest bonds would correspond to the “first” yield. According to Wang and Leung (2008a) at this stage the soil structure can accommodate the damage caused by random events by redistributing the applied stresses to the neighbouring soil (fig. 5). Afterwards, bond breakage events tend to

spread out rapidly in the bonded soil mass until a sharp decrease in soil stiffness is observed. This transition point is named as “gross” yield and herein denoted as *Y* in figure 5. As illustrated in fig 5, point *Y* occurred at an axial strain slightly less than 2.0% at which some plastic deformations appeared.

The peak stress ratio (η_{max}) and the maximum dilatancy (d_{max}) do not occur at the same axial strain and a delayed development of the maximum dilatancy is observed in both cemented samples, as illustrated in fig. 4. Inspection of fig. 6 reveals that the phenomenon of “delayed dilatancy” tends to reduce with increasing initial effective confining stresses. The strain ratio appearing on the ordinate axis of the plot is calculated as the axial strain at the peak strength divided by the strain at the point where the dilatancy achieves its maximum value (d_{max}).

After the peak strength (fig. 4), the bond-breakage events lead to a decrease in strength. Such strength degradation is more rapid in weakly cemented samples (fig. 4a) than in moderately cemented ones (fig. 4b). This evidence will be discussed in more detail in the next section.

After d_{max}, the soil strain softens, apparently following a unique straight line frictional trend on the stress-dilatancy plots (fig. 4). On the other hand, the dilatancy gradually approaches zero but critical state condition (d=0) is not always attained in all tests even when the axial strain (ε_a) is 25%.

Shear strength data for cemented and uncemented sand specimens are presented in *q-p'* plane in fig.7. As would be expected, for the uncemented loose specimens, the peak strength is found to be a straight line passing through the origin. The peak failure envelope indicates an internal friction angle of about 37°, while for weakly cemented specimens the failure envelope at peak state is slightly curved downward in the low stress region. Hence, following the proposal outlined in Lo et al. (2003),

the modeling of failure data was based on the assumption that for both cemented and uncemented sand, failure envelope can be fitted by a power function as expressed in eq (1) below:

$$q_f = A \cdot (p' + p'^{*})^m \quad (1)$$

where A, p'^{*} and m are empirical constants.

The corresponding values are:

• A=M=1.51; p'^{*}=0; m=1; correlation factor R^2=0.997 for uncemented specimens

• A=1.88; p'^{*}=27.8 kPa; m=0.97; correlation factor R^2=0.999 for cemented specimens.

The intercept cohesion c'_p on the Mohr – Coulomb (τ_{ff}-σ'_{ff}) plane resulted in 23.9 kPa with τ_{ff} and σ'_{ff} being the shear stress and the effective normal stress at failure on the failure plane, respectively.

3.3 Comparison between experimental results and stress-dilatancy relationships

It is well recognized that the shear resistance of cemented sands with no crushable grains is determined by three components including cohesion, dilatancy, and friction. With the aim of predicting the stress dilatancy behaviour in cemented sand, revised stress-dilatancy relations were proposed in literature (Lade and Overton 1989, Rowe 1962, 1963, Zhang and Salgado 2010) which can be used to describe the plastic flow of a bonded geomaterial (De Simone and Tamagnini 2005, Gao and Zhao 2012, Yu et al. 2007).

Following the work of Rowe (1962, 1963) which was based on minimum energy considerations of particle sliding for cohesive-frictional materials (e.g., cemented sands), Yu et al. (2007) derived an expression in terms of variables η and p', written from the original stress-dilatancy relationship as follows:

$$\frac{\delta\varepsilon_p^p}{\delta\varepsilon_q^p}=\frac{9(M-\eta)+6\frac{c}{p'}\sqrt{(3+2M)(3-M)}}{9+3M-2M\eta+4\frac{c}{p'}\sqrt{(3+2M)(3-M)}} \quad (2)$$

where $\delta\varepsilon_q$ is the incremental plastic deviatoric strain and η is the stress ratio q/p'. M is the slope of the critical state line under triaxial compression in q-p' space. The theoretical stress-dilatancy relationships expressed by equation (2) are plotted in figure 8 for M=1.38 (ϕ'_{cs}=35°) and for different c/p' values.

Following a different approach based on the saw-tooth model and the laws of friction of De Josselin de Jong (1976), recently Zhang and Salgado (2010) proposed a new stress-dilatancy relation for non-associated Mohr–Coulomb soils that have both cohesive and frictional strength components rewritten as:

$$d=\frac{\delta\varepsilon_p^p}{\delta\varepsilon_q^p}=\frac{9(M-\eta)-3m_c}{9+M(3-2\eta)+m_c} \quad (3)$$

m_c being a term which is related to the interparticle cohesion, c, which is given by:

$$m_c=\frac{6(3-M)(c/p')^2}{3-\eta}-\frac{2c'(3-M)}{p'}\sqrt{\left(\frac{3c'/p'}{3-\eta}\right)^2+\frac{3+2\eta}{3-\eta}} \quad (4)$$

The stress-dilatancy curves expressed from eq. (3) are also displayed in figure 8. In both cases (eq.2 and 3) it can be seen that, due to the effect of bonding, the stress-dilatancy relationships become more linear and tend to shift to the right thus reducing dilatancy at a given stress ratio, in accordance with experimental data from laboratory tests. For purely frictional behaviour (c/p'=0) the two relationships lead to a unique curve which is valid for uncemented/unbonded sands.

Figure 8 also shows stress–dilatancy data obtained from drained triaxial tests carried

out on uncemented Ticino sand at different values of $p'_{c.}$ It is evident that experimental points lay down the theoretical curve drawn for c/p'=0 and that at larger strains they gather around close to a point M =1.38 on the vertical axis, corresponding to a critical state friction angle ϕ'_{cs}=35°.

Figure 9 reports experimental data from drained TX tests performed on both weakly and moderately cemented sand at two different effective confining stresses together with theoretical stress-dilatancy relations expressed by eq. (2).

Prior to reaching the yield point, which corresponds to a significant breakage of bonding, dilatancy is inhibited by the presence of bonding between the particles of the cemented soil and the behaviour is mainly controlled by initial interparticle cohesion (c_o). Afterwards, a significant degradation of interparticle cohesion occurs, evidenced by the crossing of the experimental trend with successive theoretical curves characterized by decreased values of c/p' ratios. According to Wang and Leung (2008b), peak and post-peak phases are the net result of two competing but intimately correlated phenomena: a) decementation which results in reduction of strength and b) dilatancy which leads to an increase in strength. Up to peak strength the progressive decay of interparticle cohesion is overwhelmed by the gain in dilatancy; correspondingly, the mobilized strength tends to increase. At peak, bond breakage events are still numerous and probably concentrated within a shear band. Accordingly, volume dilation continues to develop at a reduced rate and its contribution to the mobilized strength is now overwhelmed by strength reduction associated to bonding degradation. A softening phase is then observed ((fig.9a) in which the strength reduction is accompanied by a simultaneous increase of dilatancy up to a maximum value that is reached at a point beyond the peak strength. The

smaller the confining pressure, the larger the stress-ratio achieved, and the greater the maximum rate of dilation.

In the final stage of the test, experimental points tend to align themselves with the stress-dilatancy curve of the uncemented sand and possibly attain a critical state condition at the point where the curve crosses the vertical axis. Actually a final zero volumetric strain condition was achieved only in a limited number of tests. Guided by previous findings reported by other authors (i.e. Wang and Leung 2008b), at the ultimate state the cementing bonds remain to form clusters even within the shear band. The existence of clusters not only helps maintain the overall volumetric dilation but in turn increases the associated strength. This explains why the associated measured critical-state strength can be affected by the cement content (Marri et al 2012, Rios et al 2014). The existence of such a critical state and the way it is affected by the degree of cement content should be further investigated. Nevertheless, it must be recognized that the complete determination of the ultimate or critical state in a *p'*:*q*:*e* space presents some experimental difficulties, given the brittle behavior and the strain localization observed for cemented specimens.

The delayed dilatancy phenomenon previously described is more pronounced for weakly cemented specimens (fig. 9a) than for moderately cemented ones (fig. 9b). As far as the latter are concerned, after the peak the opposite effects of bond breakages and dilatancy tend to balance each other in a more prolonged way. At large strains, all cemented sand specimens (fig. 9a and 9b) tend towards a purely frictional behavior, i.e interparticle cohesion *c* tends to have values close to 0. This is especially true the higher effective confining stress and the lower the degree of cementation.

It is apparent from the aforementioned figure that the model effectively captures the main features of the response of cemented sands during shearing. The small apparent increase in cohesion that is observed in the final portion of the curves can be attributed to the effect of strain localization (de Bono et al. 2014, Wang and Leung 2008). Another important aspect emerging from fig. 9 is the influence of effective confining stresses on the overall stress-dilatancy behaviour of tested sands. As can be seen, at comparable stress ratios the interparticle cohesion manifested by the cemented sands at higher confining stresses is lower compared to that exhibited by the lower ones. This is particularly evident for weakly cemented sands at p'_c= 200 kPa whose strength behavior appears purely frictional.

According to eq.(2), the stress–strain behaviour of cemented soils in triaxial tests depends on the relative trends of friction, dilatancy and interparticle cohesion, which are the three components of mobilized strength. Typical examples of such trends, concerning dilatancy and interparticle cohesion, are shown in figures 10a and 10b. Both figures are drawn from TX tests carried out on weakly cemented sands at two effective confining pressures. The interparticle cohesion component was back-calculated through an analytical procedure using (η,d) experimental data and the theoretical stress-dilatancy relationship expressed in eq.(2). As was pointed out previously, the initial portions of the curves are in the elastic domain that is outside the applicability range of stress-dilatancy theories. It is worthwhile mentioning that the maximum value of c, after which a pronounced bonding degradation occurs, is practically coincident with the yield point Y experimentally identified following the approach shown in fig 5. This correspondence can be considered a validation of the approach followed in the present study.

After yield, bonding degradation occurs quite suddenly in both tests which are reported in fig.10a and 10b. In both cases, the strength contribution given by the interparticle cohesion prevails at very low strains considering the fact that plastic response and associated dilatancy are hindered by cementation (Wang and Leung 2008b).

3.4 Degradation rate of interparticle cohesion

In order to describe the progressive destructuring of bonding, an exponential expression was selected linking the degradation of the interparticle cohesion (c) to the resultant of the total plastic strain vector ($\boldsymbol{\varepsilon}_d$), defined as :

$$\epsilon_d = \sqrt{(\epsilon_p^p)^2 + (\epsilon_q^p)^2} \tag{5}$$

being:

- ϵ_p^p = plastic volumetric strain $=\epsilon_1^p + 2\epsilon_3^p$ for triaxial conditions
- ϵ_q^p = plastic shear strain $=\frac{2}{3} \cdot (\epsilon_1^p - \epsilon_3^p)$ for triaxial conditions

The incremental adopted relationship, as suggested also by other authors (i.e. Yu et al. 2007) is given by the following expression:

$$\delta c = -D_c \cdot c \cdot \delta\varepsilon_d \tag{6}$$

being:

D_c =degradation rate factor

A rearranged expression resulting from integration of eq.(6) is obtained to define the degradation of the interparticle cohesion with straining, expressed as follows:

$$c = c_0 \cdot e^{-D_c \cdot (\varepsilon_{d-\epsilon_{d0}})} \quad (7)$$

where:

c_o and ε_{do} are the values of interparticle cohesion and total plastic strain, respectively, when massive bonding degradation starts to occur.

These two parameters are deduced from the analysis of TX test data based on stress dilatancy theories described above in par.[3.3]. In particular, c_o represents the maximum value of *c* determined through the aforementioned analysis in the shearing phase of tests.

Figure 11 shows typical *c* vs. ε_d best fitting curves obtained from a TX test conducted on a weakly cemented specimen consolidated at low effective confinement pressure (p'_c=20 kPa). Data points were processed by Rowe (1962,1963) and Zhang and Salgado (2010) stress-dilatancy relationships. The corresponding relevant parameters of the degradation function (eq.7) , namely c_o and D_c, are evidenced in the same figure. As can be seen, the two best-fitting curves match rather satisfactorily the trend of experimental data at low strains but they tend to diverge significantly in the final stage of the test where the interparticle cohesion tends to stabilize around a constant residual value. The agreement improves on specimens tested at higher confining pressures since residual values of "*c*" tend to progressively reduce down to zero.

In figure 12a the maximum (initial) interparticle cohesion (c_o) evaluated in all TX tests conducted on weakly cemented specimens using the previously described approaches are plotted against the effective confining pressures of the tests. In the same figure, the best fitting curves based on an exponential law are superimposed over the experimental data points. Both curves show a regular trend with a tendency of "*c*" to increase when p'_c approaches zero. Extrapolation of best fitting exponential

curves up to the vertical axis yields an approximately unique intercept point corresponding to c_0=23 kPa. Such a value should be representative of the cementation strength of the unstressed specimens. It is interesting to notice that this value of interparticle cohesion is very close to the intercept cohesion (c'=23.9 kPa) evidenced by the curved Mohr-Coulomb peak failure envelope in fig. 7.

As mentioned in par.1, the good correspondence between c_o at p'_c =0 and c' of curved Mohr- Coulomb criterion is consistent with the experimental data gathered by Lo et al. (2003) from drained TX tests at zero effective confining stress (p'_c=0) and also with the strength behaviour of bonded materials at very low confining stresses predicted on the basis of the theoretical framework proposed by Coop (2005). The latter results can be considered a further validation of the approach followed in this paper. Whilst there is inevitably some scatter of bonding degradation factor data in figure 12b, it is apparent that that bonding degradation tends to occur more rapidly with the increase of p'_c.

Conclusions

In this study an experimental investigation concerning the main features of bonding degradation of weakly cemented sand under shearing loading is presented. The study was conducted on artificially cemented silica sand samples subjected to isotropically consolidated drained TX tests carried out at different effective confining stresses (p'_c) in the range $p'c$= 20kPa to 400 kPa. Test results were interpreted in the framework of Rowe's (1962,1963) stress-dilatancy theory, using the interparticle cohesion (c) defined as a measuring parameter of the "actual" bonding shear strength. For comparison and further confirmation purposes, the stress-dilatancy

relation for cemented sands proposed by Zhang and Salgado (2010) was also adopted. The salient findings can be summarized as follows:

1) In the early shearing stage, cemented specimens exhibit an approximately elastic behaviour up to a yielding strain, at which an abrupt destructuring of the bonding network starts to occur. Prior to yielding, dilatancy is hindered by the high strength of such an intact network and the interparticle cohesion is at its highest value before decaying. This maximum value (c_o) reflects the unsheared condition of the specimen and differs from the intrinsic shearing strength of the bonded material since the first one was partially destroyed by the consolidation stage at which the specimen had been subjected. Thus, c_o will tend to decrease with the increase of the effective confining stresses of the tests (p'_c), as was ascertained in the present study.

2) After yielding, bond breakage enhances the granular nature of specimens and dilatancy tends to grow with positive effects on the mobilized strength. Meanwhile, the progressive decay of the interparticle cohesion leads to a decrease in strength. The final result is that, unlike uncemented sands, peak failure and maximum dilatancy do not occur at the same strains but the maximum dilatancy is to some extent "delayed". The delay is more pronounced as the effective confining stress of the tests decreases.

3) The results obtained show that bonding degradation tends to occur more rapidly with the increase of p'_c and, correspondingly, the interparticle cohesion at peak failure tends to reduce with the increase of p'_c. After the peak strength, most of the bond breakages have already taken place and the interparticle cohesion

tends to decrease rapidly and can even disappear completely. A low, non zero residual value of “c” was only observed in the test carried out at the lowest effective confinement stress (p'_c= 20 kPa), while for all the remaining tests a null final value (c = 0) was obtained. Nevertheless, at the ultimate state some volume dilation was still observed, probably due to some bonded clumps, which were not completely destroyed, even at this stage. This is consistent with both experimental and numerical data reported by other authors (Wang and Leung 2008b, Rios et al 2014).

4) To describe the full degradation process of bonding under shearing loading, an exponential relationship linking the interparticle cohesion to the resultant of total plastic strain tensor was adopted, as previously defined by Yu et al.(2007), and the relevant parameters were provided. The results obtained in this study display that this relationship is capable of fitting the experimental data relatively well in tests where a final zero value of the interparticle cohesion is determined (i.e. tests carried out at high effective confining stresses). When a non zero residual value is inferred (such as in the test at p'_c = 20 kPa), the agreement is less satisfactory but it improves when the regression analysis is limited to a reduced strain range.

5) The curve reporting the trend of the maximum interparticle cohesion (c_o) evaluated in each test against the effective confining pressure was extrapolated up to the p'_c =0 axis, in order to determine the initial shear strength of the bonded material (i.e. the strength of the material in the unsheared state). The interparticle cohesion assessed by the approach described above was compared with the cohesion intercept of the Mohr-Coulomb curved peak failure envelope, and a good correspondence, namely 23 kPa against 23.9 kPa, was obtained between the two parameters. This finding is consistent with other evidence reported in

literature (i.e. Coop 2005, Lo et al. 2003) but further confirmation will be required through new research based on a broader range of cementing agents and cementation strengths.

References

ASTM (2011) D 4767-11. Standard test m method for consolidated undrained triaxial compression test for cohesive soils. ASTM International, West Conshohocken, PA, USA.

Baudet, B. and Stallebrass, S., 2004. A constitutive model for structured clays. *Géotechnique* 54(4), 269—278 [doi:10.1680/geot.2004.54.4.269].

Clough, G.W. and Sitar, N., 1981. Cemented sands under static loading. *Journal of Geotechnical Engineering ASCE*, 107(GT6), 799–817.

Consoli, N.C., Cruz, R.C., Viana da Fonseca, A. and Coop, M.R., 2012. Influence of cement-voids ratio on stress-dilatancy behavior of artificially cemented sand. *J. Geotech. Geoenviron. Eng. ASCE,* 138(1), 100-109 [doi: 10.1061/(ASCE)GT.1943-5606.0000565].

Coop, M.R. and Atkinson, J.H., 1993. The mechanics of cemented carbonate sands. *Géotechnique*, 43, 53–67.

Coop, M.R. and Willson, S.M., 2003. Behavior of hydrocarbon reservoir sand and sandstones. *J. Geotech. Geoenviron. Eng. ASCE*, 129(11), 1010–1019.

Coop, M.R.,2005. On the mechanics of reconstituted and natural sands. In: Di Benedetto *et al*., eds. *Proceedings of Deformation Characteristics of Geomaterials*. Taylor & Francis Group, London,29-58.

Cuccovillo, T. and Coop, M.R., 1993. The influence of bond strength on the mechanics of carbonate soft rocks. In: A. Anagnostopoulos, R. Frank, N. Kalteziotis, and F.Schlosser eds. *Proceedings of 1st Int. Symp. on the Geotechnics of of Hard Soils–Soft Rocks*, Balkema, Rotterdam, vol. 1, 447-455.

Cuccovill,o T. and Coop, M.R., 1997. Yielding and pre-failure deformation of structured sands. *Géotechnique,* 47(3), 491–508.

Cuccovillo, T. and Coop, M.R., 1999. On the mechanics of structured sands. *Géotechnique*, 49(6),741–760.

De Bono, J., McDowell, G. and Wanatowski, D., 2014. Investigating the micro mechanics of cemented sand using DEM . *J. Numer. Anal. Meth. Geomech*., 39(6), 655-675 [doi:10.1002/nag.2340].

De Josselin De Jong, G. 1976. Rowe's stress–dilatancy relation based on friction.

Géotechnique, 26(3),527–534.

DeSimone, A. and Tamagnini,C., 2005. Stress–dilatancy based modelling of granular materials and extensions to soils with crushable grains. *J. Numer. Anal. Meth.*, 29, 73–101 [doi: 10.1002/nag.405].

Gens, A. and Nova, R., 1993. Conceptual bases for a constitutive model for bonded soils and weak rocks. *Proceedings of an International Symposium under the auspices of the ISSMFE on Geotech. Eng. hard soils-soft rocks*, 20-23 September 1993, Athens, Greece **,** 1(1), 485-494.

Gao, Z. and Zhao, J., 2012. Constitutive modeling of artificially cemented sand by considering fabric anisotropy. *Computers and Geotechnics*, 41, 57–69.

Hamidi, A. and Haeri, S.M., 2008. Stiffness and deformation characteristics of cemented gravely sands. Int. J. of Civil Engineering, 6(3),159-173.

Huang, J.T. and Airey, D., 993. Effects of cement and density on an artificially cemented sand. In: A. Anagnostopoulos, R. Frank, N. Kalteziotis and F. Schlosser eds. *Proceedings of 1st Int. Symp. on the Geotechnics of of Hard Soils–Soft Rocks*, Balkema, Rotterdam, vol.1, 553–560.

Ismail, M.A., Joer, H.A., Sim. W.H. and Randolph, M.F., 2002. Effect of cement type on shear behaviour of cemented calcareous soil. *J. Geotech. Geoenviron. Eng ASCE***,** 128(6), 520-529.

Lade, P.V. and Overton, D.D., 1989. Cementation effects in frictional materials. *J. Geotech. Engrg. ASCE*, 115 (10), 1373–1387.

Lagioia, R. and Nova, R., 1995. An experimental and theoretical study of the behaviour of a calcarenite in triaxial compression. *Géotechnique,* 45(4), 633–648.

Leroueil, S. and Vaughan, P.R.,1990. The general and congruent effects of structure in natural soils and weak rocks. *Géotechnique*, 40(3),67–488.

Lo, S.C.R., Lade, P.V. and Wardani, S. P.R. (2003) An Experimental Study of the mechanics of two weakly cemented soils. *Gèotechnical Testing Journal*, 26(3), Paper ID GTJ10405_263, 1-14.

Malandraki, V. and Toll, D.G., 2001. Triaxial tests on weakly bonded soil with changes in stress path. *J. Geotech. Geoenviron. Eng ASCE,* 127(3), 282–291.

Marri, A., Wanatowski, D. and Yu, H.S., 2012. Drained behavior of cemented sand in high pressure triaxial compression tests. *Geomechanics and Geoengineering: An International Journal*, 7(3),159-174 [doi: 10.1080/17486025.2012.663938].

Nova, R., Castellanza, R. and Tamagnini, C.,2003. A constitutive model for bonded geomaterials subject to mechanical and/or chemical degradation. *Int. J. Numer. Anal. Meth. Geomech.*, 27, 705–732 [doi:10.1002/nag.294].

Porcino, D. Marcianò, V. and Granata, R.,2011. Undrained cyclic response of a silicate-grouted sand for liquefaction mitigation purposes. *Geomechanics and Geoengineering An International Journal*, 6(3), 155-170 [doi:10.1080/17486025.2011.560287].

Porcino, D. Marcianò, V. and Granata, R., 2012. Static and dynamic properties of a lightly cemented silicate-grouted sand. *Canadian Geotechnical Journal*, 49 (10), 1117-1133 [doi: 10.1139/t2012-069].

Porcino, D., Marcianò, V. and Granata, R.,2015. Cyclic liquefaction behaviour of a moderately cemented grouted sand under repeated loading. *Spoil Dynamics and Earthquake Engineering*, 79 Part A,36–46 [doi:10.1016/j.soildyn.2015.08.006].

Reddy, K.R. and Saxena, S.K., 993. Effects of cementation on stress strain and strength characteristics of sand. *Soils and Foundations***,** 33(4),121–134.

Rios, S., Viana da Fonseca, A. and Baudet, B.A., 2014. On the shearing behaviour of an artificially cemented soil. *Acta Gèotechnica*, 9(2), 215–226 [doi:10.1007/s11440-013-0242-7].

Rotta, G.V., Consoli, N.C., Prietto, P.D.M. and Graham, J.,2003. Isotropic yielding in an artificially cemented soil cured under stress. *Géotechnique*, 53(5), 493-501.

Rouainia, M. and Wood, M.D.2000. A kinematic hardening constitutive model for natural clays with loss of structure. *Géotechnique*, 50(2),153164.

Rowe, P.W., 1962. The stress-dilatancy relation for static equilibrium of an assembly of particles in contact. *Proc. Series of the Royal Society of London Series A, Mathematical and Physical Sciences*, 269(1339), 500-527 [doi: 10.1098/rspa.1962.0193].

Rowe, P.W.1963. Stress-dilatancy, earth pressure, and slopes. *J. Soil Mech. Found. Div. ASCE*, 89(SM3), 37-61.

Schnaid, F., Prietto, P.D.M. and Consoli, N.C., 2001. Characterization of cemented sand in triaxial compression. *J. Geotech. Geoenviron. Eng ASCE*, 127 (10), 857-868.

Vatsala, A., Nova, R. and Murthy, B., 2001. Elastoplastic model for cemented soils. *J. Geotech. Geoenviron. Eng. ASCE*, 127(8), 679-687.

Vaughan, P.R., 1985. Mechanical and Hydraulic Properties of In-Situ Residual Soils. In:Brazilian Society for Soil Mechanics ed. *Proceedings of the 1st International Conference on Geomechanics in Tropical Lateritic and Saprolitic Soils,* A.A Balkema, Rotterdam, the Netherlands. vol. 3,231–263.

Wang, Y.H. and Leung, S.C., 2008a. A particulate-scale investigation of cemented sand behavior. *Canadian Geotechnical Journal*, 45(1), 29–44.

Wang, Y.H. and Leung, S.C.,2008b. Characterization of cemented sand by experimental and numerical investigations. *J. Geotech. Geoenviron. Eng ASCE*, 134(7), 992-1004.

Yu, H.S., Tan, S.M. and Schnaid, F., 2007. A critical state framework for modelling bonded geomaterials. *Geomechanics and Geoengineering: An International Journal,* 2(1), 61-74 [doi:10.1080/17486020601164275].

Yu, H.S., Khong, C.D., Wang, J. and Zhang, G., 2005. Experimental evaluation and extension of a simple critical state model for sand. *Granular Matter* 7(4), 213–225 [doi: 10.1007/s10035-005-0209-y].

Zhang, J. and Salgado, R., 2010. Stress–dilatancy relation for Mohr–Coulomb soils following a non-associated flow rule. Technical Note. *Géotechnique* 60(3), 23–226 [doi:10.1680/geot.8.T.039].

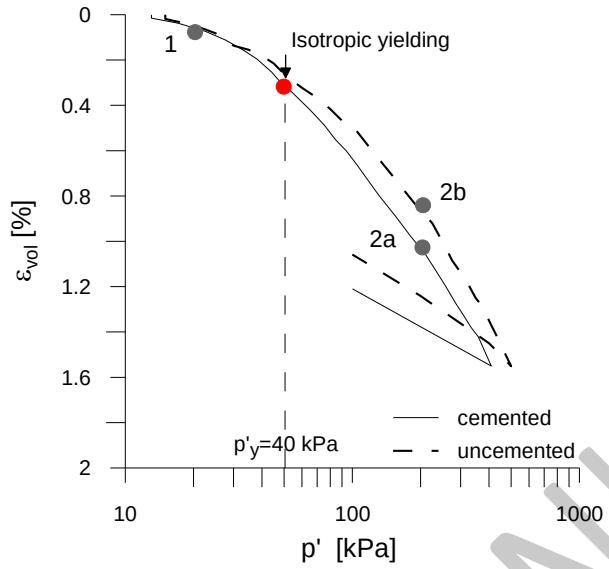

(a)

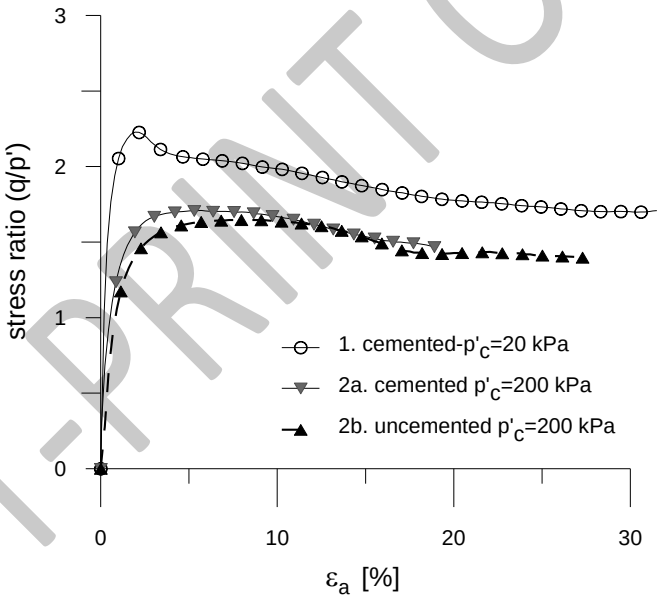

(b)

Figure 1.Typical patterns of (a) isotropic compression and (b) stress-strain curves of weakly cemented specimens

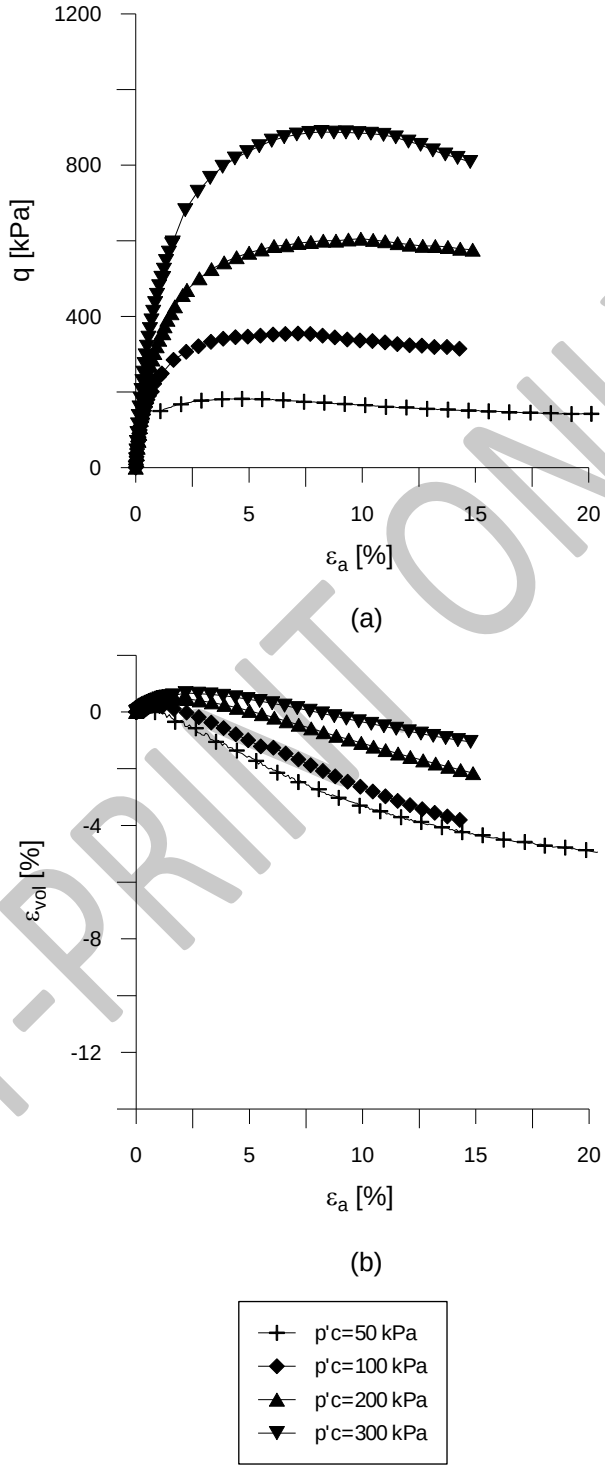

Figure 2.Stress–strain–volumetric response of uncemented TS sand samples.

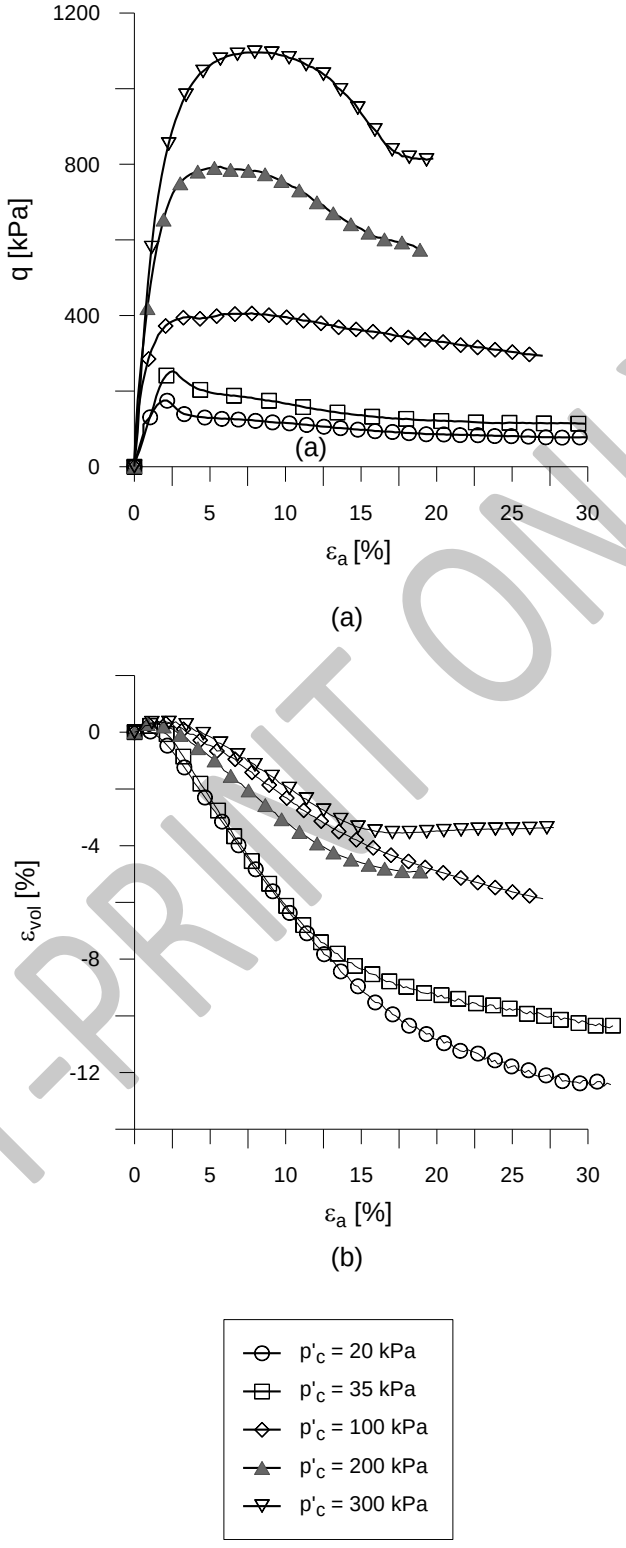

Figure 3.Stress–strain–volumetric response of weakly cemented TS sand samples.

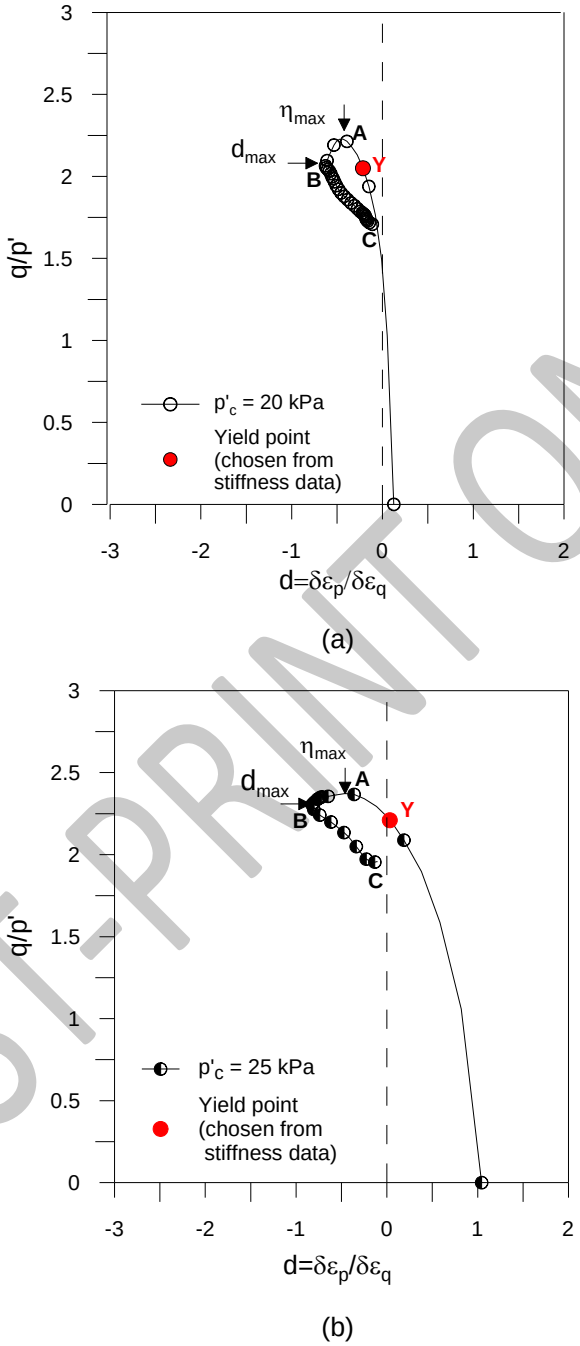

Figure 4. Experimental Stress-dilatancy relationships for cemented TS samples at low effective confining stress: (a) weakly and (b) moderately.

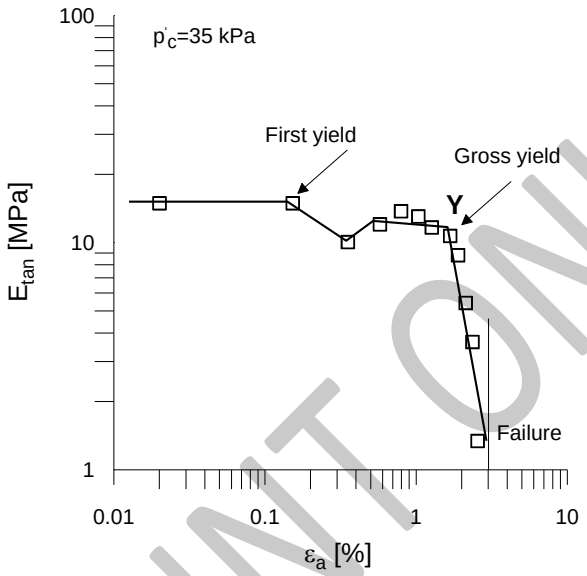

Figure 5. Definition of "first" and "gross" yield points in logarithmic stiffness-strain curve for weakly cemented specimens.

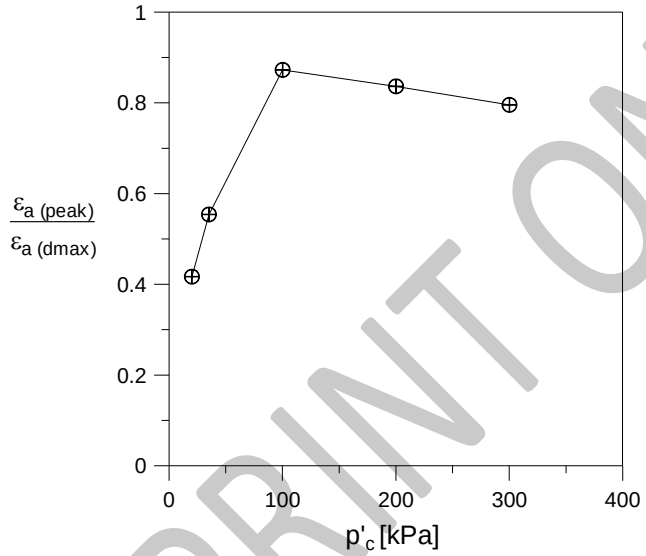

Figure 6. Influence of effective confining stress on "delayed maximum dilatancy" of weakly cemented samples in TX tests.

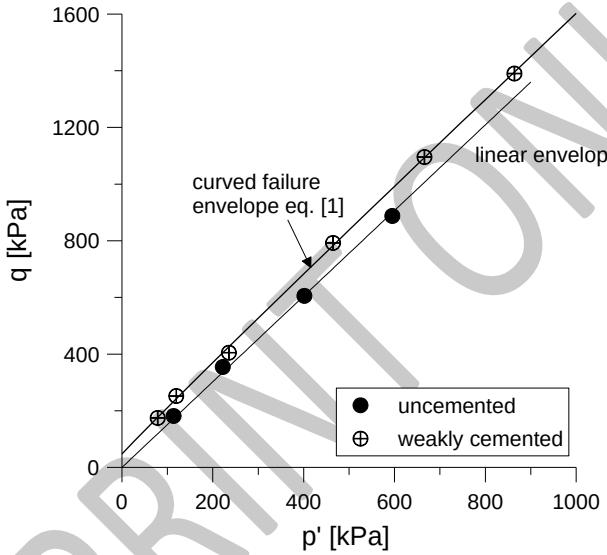

Figure 7. Failure envelopes for cemented and uncemented TS sand samples.

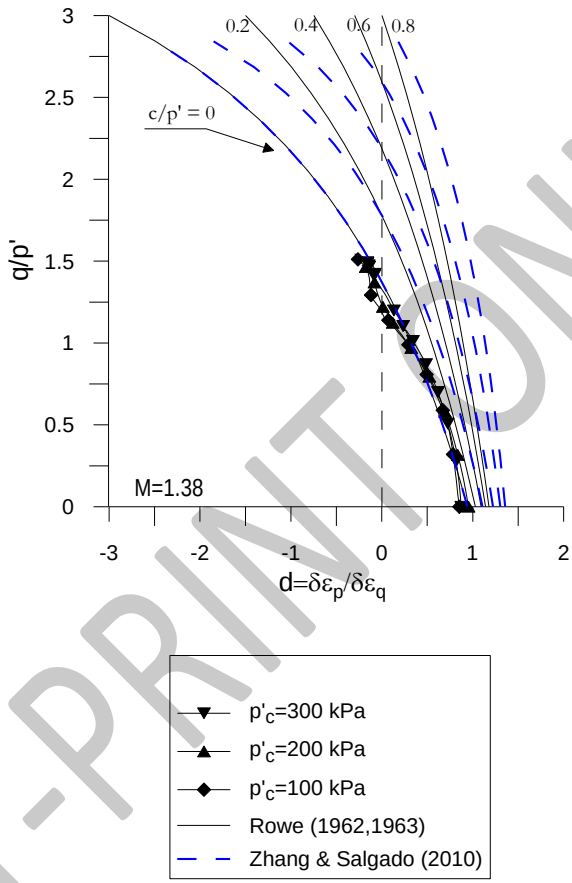

Figure 8. Theoretcical **s**tress–dilatancy curves following two different approaches and experimental TX data of uncemented TS samples (loose).

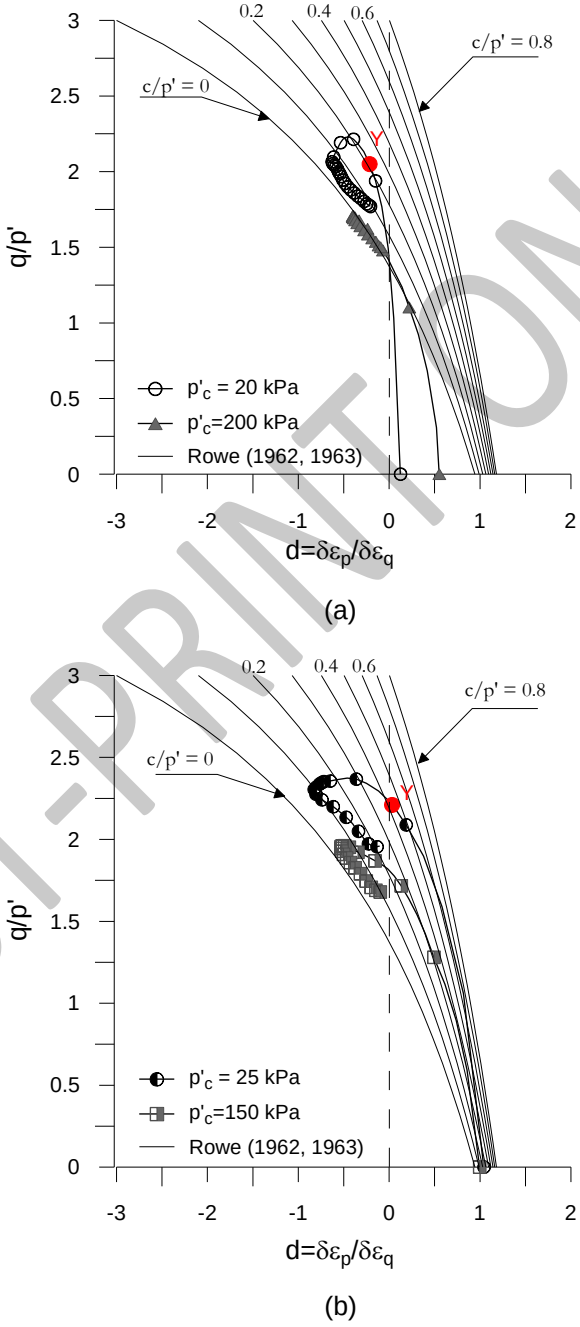

Figure 9. Influence of different effective confining stresses on stress-dilatancy relationships for TX tests on (a) weakly and (b) moderately cemented TS samples.

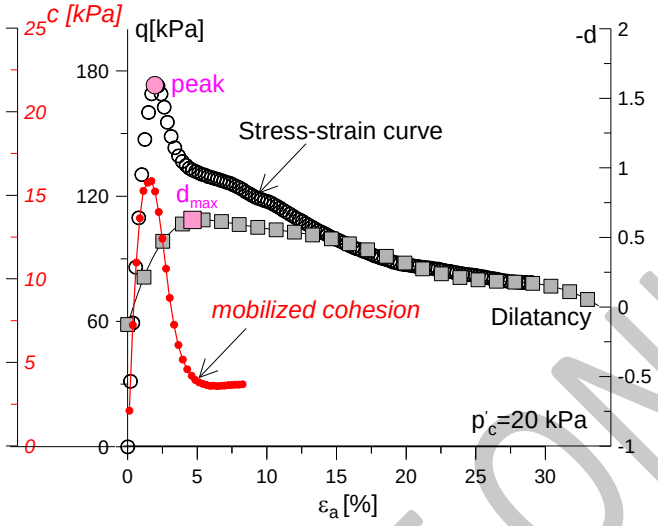

(a)

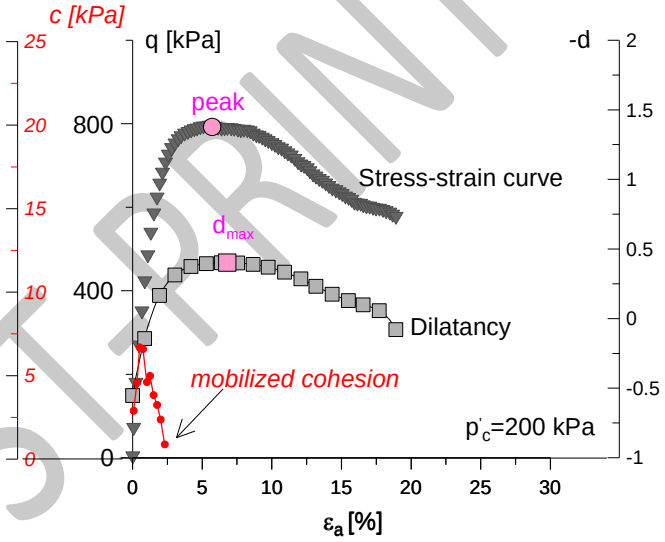

(b)

Figure 10. Stress-strain curve, trend of dilatancy and interparticle cohesion in TX tests for weakly cemented TS sand samples sheared at low (a) and high (b) effective confining stresses.

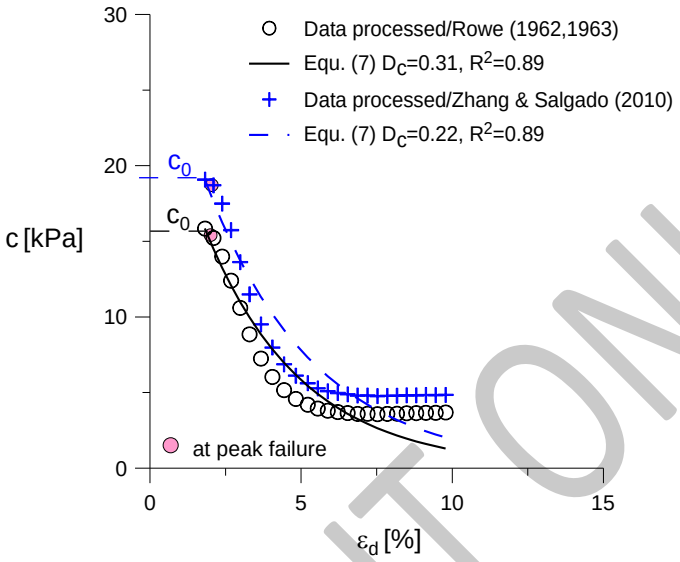

Figure 11 Degradation curve of interparticle cohesion with total plastic strains (ε_d) of weakly cemented sand samples during shearing (p'_c=20 kPa).

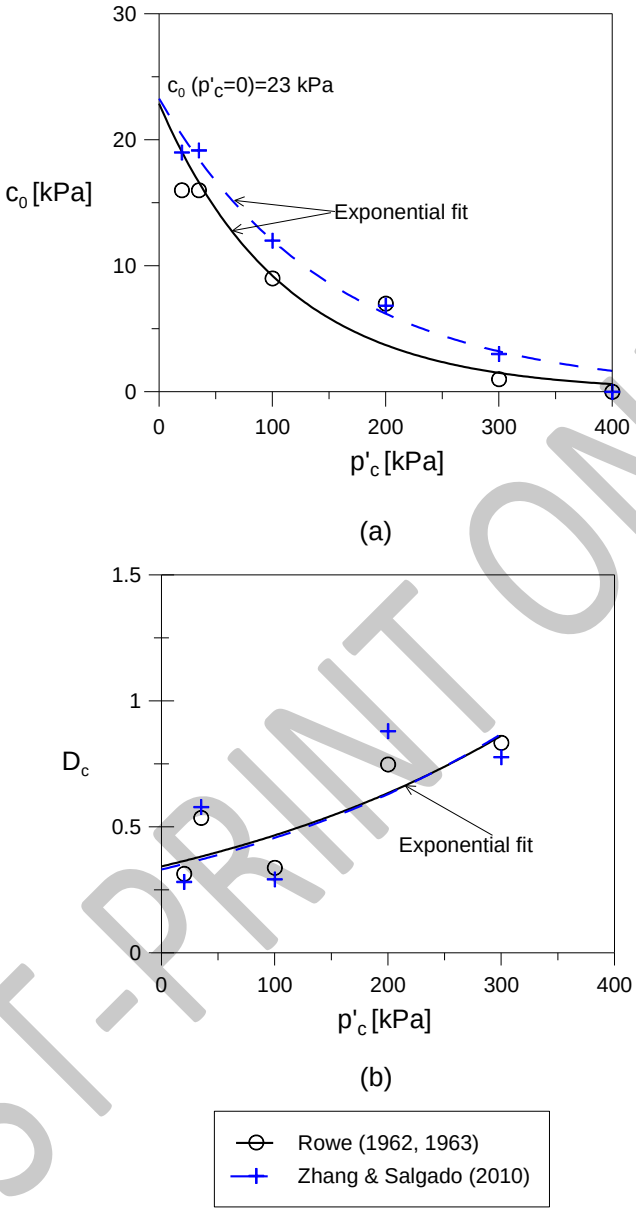

Figure 12 Trend of (a) maximum interparticle cohesion and (b) bonding degradation coefficient (D_c) with mean effective confining stress in TX tests for weakly cemented specimens .

Table 1. Index properties of Ticino silica sand

Parameter		*Mineralogical composition*	
γ_{max} [kN/m^3]	16.67	Quartz [%]	30
γ_{min} [kN/m^3]	13.64	Feldspar [%]	65
G_s	2.68	Mica [%]	5
U_c	1.3		
D_{50} [mm]	0.6		